Oscillations in arid alluvial-channel geometry

Jon D. Pelletier
Stephen DeLong
Department of Geosciences, University of Arizona, 1040 East Fourth Street, Tucson, Arizona 85721, USA

ABSTRACT

Arid alluvial channels on piedmonts and valley floors often exhibit an oscillating pattern of narrow, deeply incised reaches and wide, shallow reaches with a characteristic wavelength. How do these oscillations develop and what controls their wavelengths? To address these questions we developed a two-dimensional numerical model that couples erosion and deposition in a channel bed with cross-sectional widening and narrowing. This model is inherently unstable over a range of spatial scales dependent on the channel width, depth, and slope. In the initial phase of model evolution, wider-than-average channel reaches become zones of distributary flow that aggrade, lose stream power, and further widen in a positive feedback. Simultaneously, narrower-than-average reaches incise, gain stream power, and further narrow. In the second stage of model evolution, this instability is balanced by the diffusive nature of longitudinal profile evolution, and solitary topographic waves propagate in the upstream direction with a characteristic wavelength and amplitude. The model predicts a specific quantitative relationship between the oscillation wavelength and channel width, depth, and slope that is verified by a database of channel geometries in southern Arizona.

Keywords: channel geometry, numerical modeling, instability, arroyo, Arizona.

INTRODUCTION

Many fluvial-geomorphic studies have modeled longitudinal-profile evolution, but in these studies, channels have most often been assumed to be uniform in width or a simple function of upstream drainage area (e.g., Slingerland and Snow, 1987; Begin et al., 1981; Sinha and Parker, 1996; Dade and Friend, 1998). Actual channels often vary substantially in width, and these variations may strongly influence channel evolution. Schumm and Hadley (1957), for example, developed their conceptual ''arid cycle of erosion'' on the basis of the episodic cut-and-fill histories and oscillating geometries observed in the arroyos of the American West. In their model, channels aggrade and widen until a threshold slope and/or width is reached, initiating incision in the oversteepened reach and aggradation in the downstream reach. Schumm and Hadley's model has not been clearly linked with established process models, however, and it remains unclear precisely how arroyos form and evolve (Reid, 1994). Bull (1997) summarized research on the behavior of arid alluvial channels, including valley-floor arroyos and piedmont discontinuous ephemeral streams. Bull emphasized the role of human disturbance and climate change in controlling the evolution of these oscillating-channel systems, but his approach does not describe how oscillations develop or what controls their wavelengths.

Oscillating alluvial channels in southern Arizona are classified as one of three basic types depending on their geomorphic position. Piedmont channels fed by montane drainage basins are continuous channels that alternate between braided and narrowly entrenched reaches with wavelengths on the order of 1 km. Wild Burro Wash on the Tortolita Piedmont is a classic example of this type of oscillating channel (Field, 2001) (Fig. 1A). Channel width (measured from 1-m-resolution U.S. Geological Survey digital orthophotoquadrangles [DOQQs]) and bed elevation (measured from a high-resolution digital elevation model [DEM] with average channel slope subtracted) in Wild Burro Wash are plotted in Figure 1A. These data illustrate that oscillations in both bed elevation and channel width occur in Wild Burro Wash and that the two oscillations are in phase.

The second type of oscillating channel is the piedmont discontinuous ephemeral stream. These channels are fed only by local piedmont runoff, and they alternate between incised channels and sheet-flow–dominated channel fans without well-defined banks (Bull, 1997). The transitions between channel fans and incised reaches occur abruptly at one or more steep ''headcuts'' (Fig. 1B). Dead Mesquite Wash in southeast Tucson is the classic example given by Bull (1997) (Fig. 1B). Packard (1974) documented in-phase oscillations in bed elevation and width in Dead Mesquite Wash, similar to the behavior of Wild Burro Wash.

The third type of oscillating channel is the classic southwestern valley-floor arroyo. These systems alternate between narrow, deeply incised channels and broad, shallow channel fans, but they typically drain one or more broad basins and adjacent ranges and have wavelengths on the order of 10 km. Abrupt headcuts also characterize distributary-to-tributary transitions in these systems. In contrast to the other oscillating-channel types, not all arroyos are periodically alternating; some are tectonically controlled by the elevations of basin divides. Cooke and Reeves (1976) identified Vamori Wash in southern Arizona as perhaps the best example of an oscillating arroyo system (Fig. 1C). Entrenched reaches are associated with low vegetation density, whereas channel fans support a broad, dense riparian zone in Vamori Wash.

The common oscillatory pattern in these channel types suggests a common underlying mechanism that acts across multiple spatial scales. This paper explores this hypothesis in two ways. First, a numerical model for the coupled evolution of the channel longitudinal profile and cross section is presented. This model predicts that arid alluvial channels are unstable over a range of wavelengths controlled by channel width, depth, and slope. Second, a database of channel geometries in southern Arizona is constructed that confirms the model predictions and places the three channel types within a single continuum, from steep, small-wavelength–oscillating channels to gently sloping, long-wavelength–oscillating channels.

MODEL DESCRIPTION

Exner's equation (conservation of mass) states that erosion and deposition in the alluvial-channel bed is proportional to the gradient of total sediment discharge, or

$$\frac{\partial h}{\partial t} = -\frac{1}{C_0}\frac{\partial (w q_s)}{\partial x}, \tag{1}$$

where h is the elevation of the channel bed, t is time, C_0 is the volumetric concentration of bed sediment, w is the channel width, q_s is the specific sediment discharge (i.e., the sediment discharge per unit channel width), and x is the distance downstream. In most bed-load transport relations, specific sediment flux is proportional to the 3/2-power of the bed shear stress. This implies that specific sediment discharge is a linear function of channel gradient and a nonlinear function of the discharge per unit channel width, or

$$q_s = -B\left(\frac{Q}{w}\right)^b \frac{\partial h}{\partial x}, \tag{2}$$

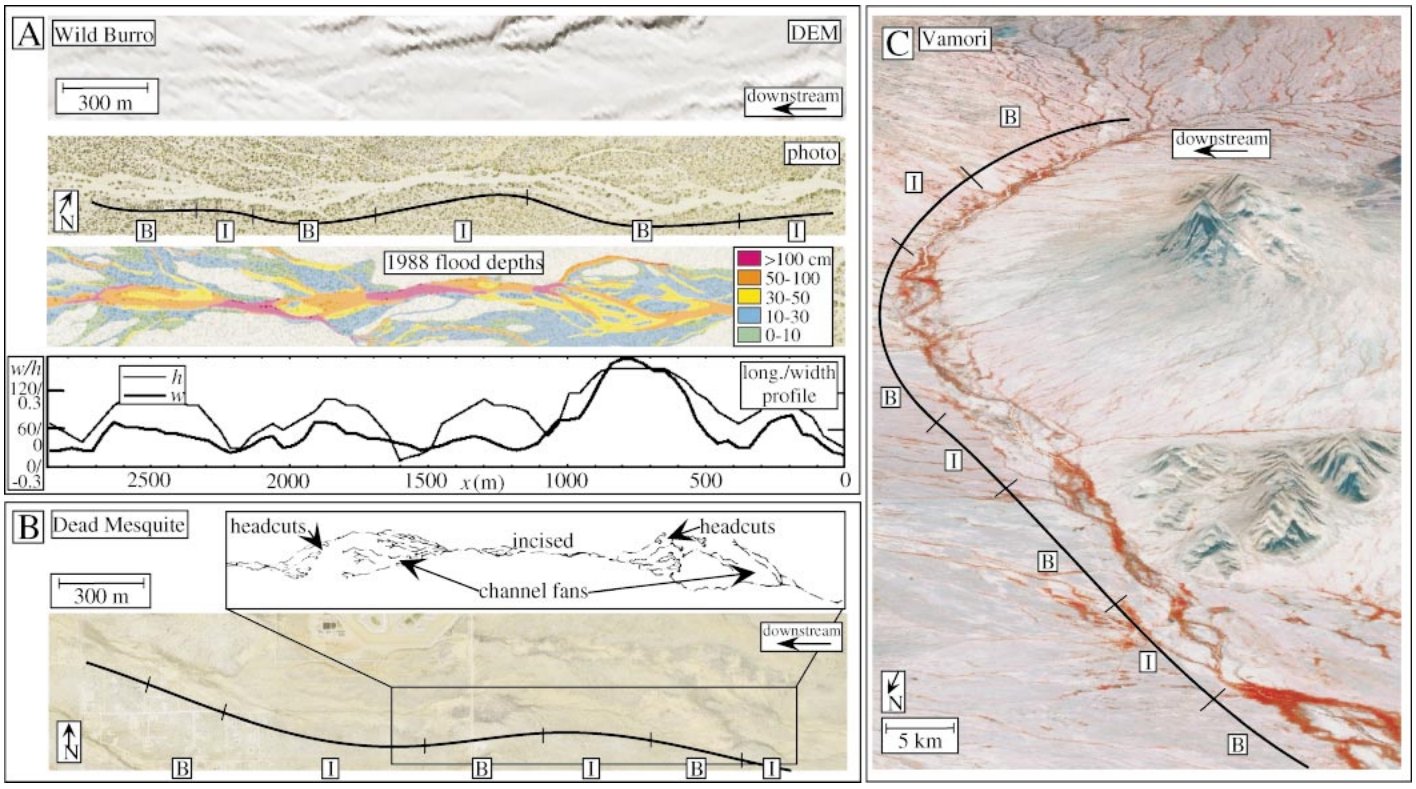

Figure 1. Examples of oscillating channels in southern Arizona. Alternating reaches: B—braided and I—incised. A: Wild Burro Wash data, including (top to bottom) high-resolution digital elevation model (DEM) in shaded relief (Pima Association of Governments, 2000), color digital orthophotoquadrangle (DOQQ), 1:200-scale flow map corresponding to extreme flood on 27 July 1988 (House et al., 1991), and plot of channel width *w* (thick line) and bed elevation *h* (thin line, extracted from DEM and with average slope removed). B: Dead Mesquite Wash shown in color DOQQ and detailed map of channel planform geometry (after Packard, 1974). C: Vamori Wash shown in oblique perspective of false-color Landsat image (vegetation [band 4] in red) draped over a DEM. Channel locations in Figure 3A.

where B is a mobility parameter related to grain size and, Q is water discharge. The value of b is constrained by sediment rating curves and is between 2 and 3 for both suspended-load and bed-load transport. Here I consider the case $b = 2$. Equation 2 assumes that the bed shear stress is much larger than the threshold for particle entrainment.

If the channel width is assumed to be uniform along the longitudinal profile, the combination of equations 1 and 2 gives the classic diffusion equation:

$$\frac{\partial h}{\partial t} = \kappa \frac{\partial^2 h}{\partial x^2}, \tag{3}$$

where the diffusivity is given by $\kappa = (BQ^2)/(C_0 w_0)$; w_0 is the uniform channel width.

If the channel width is not uniform along the longitudinal profile, the chain rule must be used when differentiating q_s in equation 1. This approach introduces an additional nonlinear term into equation 3, to give

$$\frac{\partial h}{\partial t} = \kappa w_0 \left(\frac{1}{w} \frac{\partial^2 h}{\partial x^2} - \frac{1}{w^2} \frac{\partial w}{\partial x} \frac{\partial h}{\partial x} \right). \tag{4}$$

It is convenient to define h as the difference between the local bed elevation and that of a straight, equilibrium channel with uniform discharge. Equation 4 then becomes

$$\frac{\partial h}{\partial t} = \kappa w_0 \left[\frac{1}{w} \frac{\partial^2 h}{\partial x^2} + \frac{1}{w^2} \frac{\partial w}{\partial x} \left(S_0 - \frac{\partial h}{\partial x} \right) \right], \tag{5}$$

where S_0 is the equilibrium channel slope. Equation 5 can be used to study the evolution of perturbations from the equilibrium geometry.

Channel widening and narrowing occur by a complex set of processes, including bank retreat and bed scouring. Scouring often leads to channel narrowing as flow is focused into the scour zone and parts of the former channel bed effectively become part of the bank. Bull's (1979) ''threshold-of-critical-power'' concept can be used to relate the rate of channel widening and narrowing with the excess stream power if channels are assumed to widen as they aggrade and narrow as they incise. Bull's model states that channels incise if the stream power is greater than a threshold value and aggrade if the stream power is less than that value. Expressing this relationship in terms of channel widening (aggradation) and narrowing (incision) gives

$$\frac{\partial w}{\partial t} = -\frac{w q_s - w_0 q_{s_0}}{h_0 - h}, \tag{6}$$

where q_{s_0} is the equilibrium sediment flux or stream power, and h_0 is the equilibrium bank height. Equation 6 represents a cross-sectional mass balance: sediment removed from the bank contributes to the local sediment-flux deficit $wq_s - w_0 q_{s_0}$ (i.e., the amount of sediment that cannot be transported out of the reach), promoting further aggradation in the reach.

The nonlinear term in equation 5 alters the dynamics of channels markedly compared to the diffusive behavior expressed in equation 3. Along a reach with uniform discharge and grain size, the diffusion equation smoothes out curvatures in the profile over time. The nonlinear term in equation 5, however, has the opposite effect through a positive feedback between channel width and slope. In this feedback,

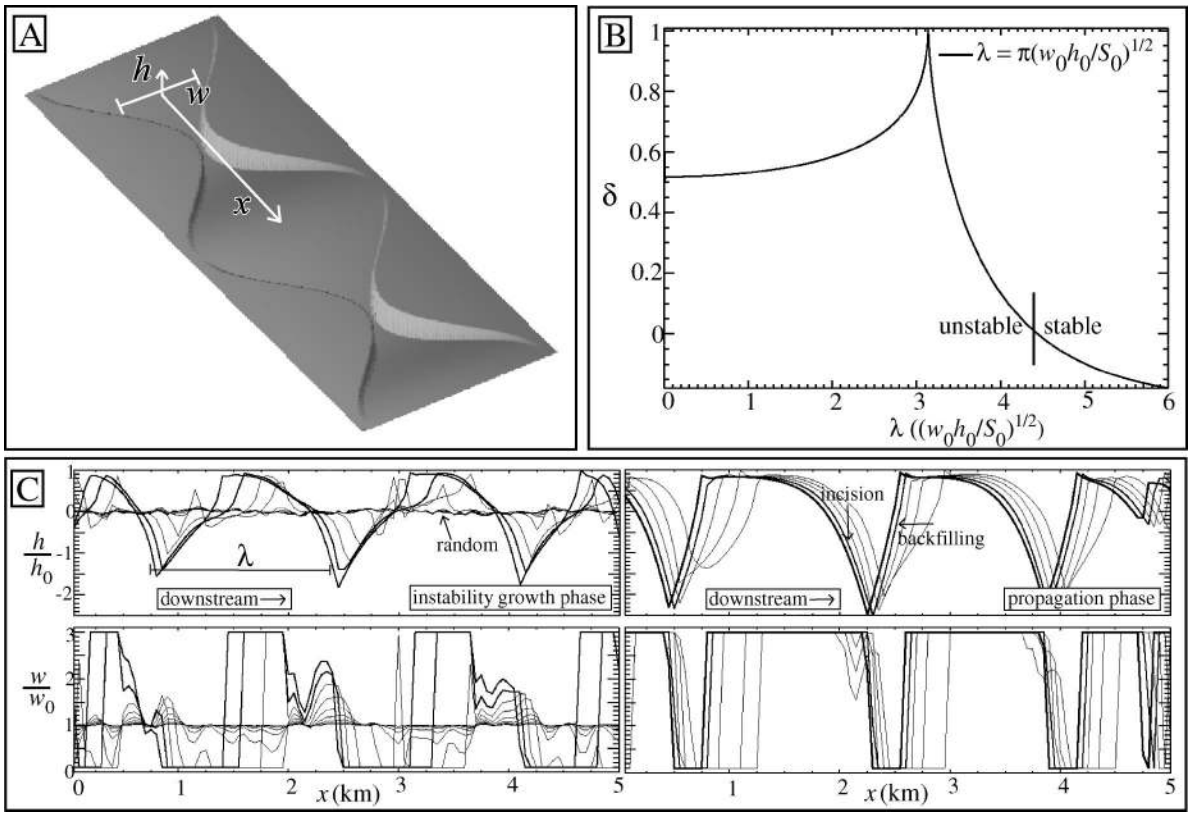

Figure 2. Model behavior. A: Schematic diagram of model geometry. B: Growth curve for linear-stability analysis, where δ is nondimensional growth rate. This analysis predicts unstable behavior for small wavelengths, with maximum value at $\lambda = \pi(w_0h_0/S_0)^{1/2}$. C: Numerical solution. Initial phase (left) is characterized by growth of small, random perturbations and increase in oscillation wavelength with time (line thickness increases with time). Steady-state phase (right) is characterized by solitary-wave propagation of oscillations in upstream direction. Incision and channel narrowing on leading edge of each wave are balanced by backfilling and widening on trailing edge.

spatial variations in channel slope generate variations in width via equation 6. Large gradients in channel width, in turn, increase the nonlinear behavior in equation 5, further localizing erosion and deposition to complete the feedback cycle. This cycle is balanced by the diffusive term, and the balance between these two terms controls the oscillation wavelength.

MODEL BEHAVIOR

Equations 5 and 6 may be solved by using linear-stability analysis and direct numerical solution. Linear-stability analysis works by solving the linear approximation to equations 5 and 6 for the growth rate of a small-amplitude oscillation superimposed on the initial channel geometry (a channel with specified equilibrium width, w_0, bank height, h_0, and slope, S_0). This analysis is presented in Appendix DR1[1] and predicts the growth curve shown in Figure 2B. The growth rate is positive (i.e., perturbations are unstable) for small wavelengths, rises to a steep maximum at

$$\lambda = \pi\sqrt{\frac{w_0h_0}{S_0}}, \tag{7}$$

and quickly becomes negative (i.e., perturbations decay to zero) for larger wavelengths. The growth rate is a function of κ (i.e., channels with larger values of κ develop oscillations more rapidly), but the wavelength corresponding to the maximum growth rate (equation 7) is independent of κ. This independence is important for testing equation 7 because κ is not well constrained, but the average channel width, bank height, and slope can be readily measured for any channel.

The two-step Lax-Wendroff scheme (e.g., Press et al., 1992) was used to integrate equations 5 and 6 for the direct numerical solution. The width was not allowed to go below 10 m or above 300 m in the model. Without bounds, the model develops infinitely small and large channel widths that are unrealistic. The model results are not sensitive to the specific values of the lower and upper bounds as long as they are small and large compared to the equilibrium channel width.

Figure 2C shows plots of bed elevation *h* (top) and channel width *w* (bottom) for the early (left) and late (right) stages of the numerical model. We assumed an initial width, bank height, and slope of 100 m, 2 m, and 0.01, respectively, with small (1%) random variations superimposed on the initial channel width. The solutions are plotted for a temporal sequence, with thicker lines representing later times. The early stage of the model is characterized by the amplification of spatial variations in width within a range of wavelengths close to 1 km. In the latter stage, oscillations achieve a steady-state amplitude and propagate upstream as a train of solitary (i.e., nondispersive) topographic waves. At any given instant, the channel geometry is characterized by alternating zones of narrow, deeply incised reaches and wide, shallow reaches. The most abrupt slope break is where the channel changes from distributary to incised. This break is similar to the headcuts often observed in arroyos and discontinuous ephemeral streams. The basic two-step model evolution is a robust feature of the model and was observed for a wide range of model parameters.

As the instability develops from random initial conditions, the dominant wavelength increases, and the channel geometry becomes

[1]GSA Data Repository item 2004117, Appendix DR1, linear-stability analysis and channel database, is available online at www.geosociety.org/pubs/ft2004.htm, or on request from editing@geosociety.org or Documents Secretary, GSA, P.O. Box 9140, Boulder, CO 80301-9140, USA.

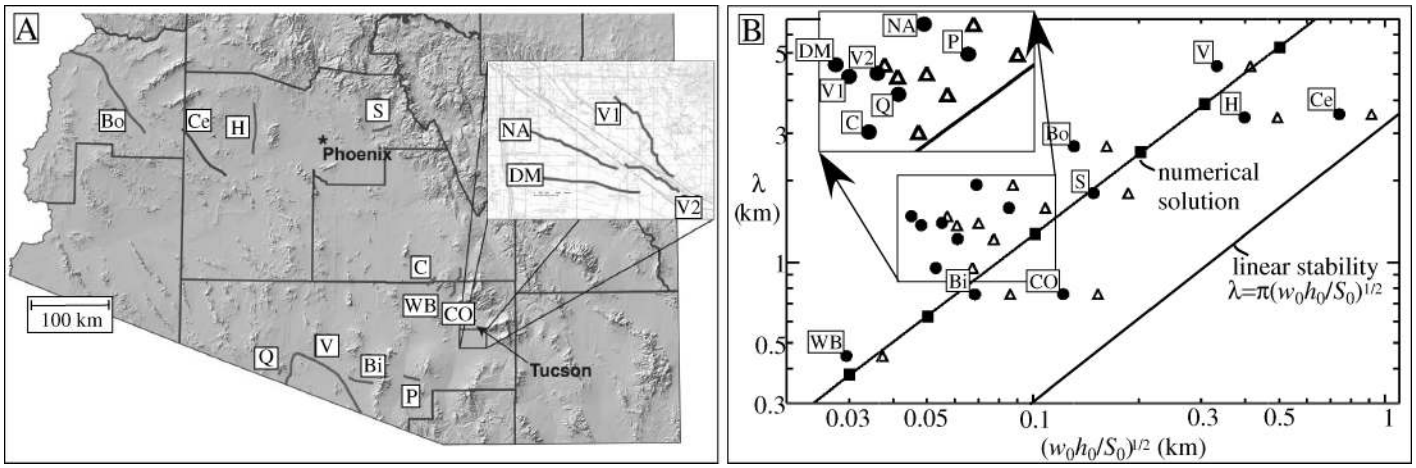

Figure 3. Database of oscillating channel geometries in southern Arizona. A: Location map. Clockwise from upper left: Bo—Bouse Wash; Ce—Centennial Wash; H—Hassayampa River; S—Sycamore Creek; NA—North Airport Wash; V1—Vail Wash; V2—Vail–Dead Mesquite Wash; DM—Dead Mesquite Wash; C—Cottonwood Wash; WB—Wild Burro Wash; CO—Canada del Oro Wash; P—Penitas Wash; Bi—Bobaquivari Wash; V—Vamori Wash; Q—East La Quituni Wash. B: Plot of oscillation wavelength λ vs. $(w_0h_0/S_0)^{1/2}$. Lower line is linear-stability prediction. Upper line and filled squares are numerical results. Observed data for channels in Figure 3A are plotted with circles (10 yr flood depth) and open triangles (25 yr flood depth).

more regularly periodic. The increase in oscillation wavelength indicates that nonlinear, finite-amplitude effects are an important part of the model behavior. This result is confirmed by Figure 3B, which compares the oscillation wavelengths predicted by the linear-stability analysis and the direct numerical solution for different values of $(w_0h_0/S_0)^{1/2}$. The lower solid line corresponds to the linear-stability prediction (equation 7), and the filled squares and upper solid line are the fully-nonlinear numerical results. Which model is more consistent with observations: the linear or nonlinear model?

EMPIRICAL DATA FOR OSCILLATING CHANNELS IN SOUTHERN ARIZONA

To test the model predictions for oscillation wavelength, we constructed a geographic information system database of DOQQs, rectified false-color Landsat imagery, and 30-m-resolution DEMs for all of southern Arizona. This database was used to measure oscillation wavelengths and average channel widths, depths, and slopes for 15 oscillating channels (Appendix DR1, see footnote 1). Our data set includes examples of each of the three channel types, including channels over a broad range of sizes. DOQQs were found to be especially useful for measuring channel widths and oscillation wavelengths in small channels, and false-color Landsat imagery was useful for distinguishing vegetation patterns associated with large arroyo oscillations.

Bank heights are difficult to estimate in many of these systems, particularly along channel-fan reaches where banks are not well defined. As an alternative to direct measurements of bank height, we estimated the average bank height using an indirect method. First, a regional frequency-discharge relationship (Thomas et al., 1997) was used to estimate a bankfull discharge for each channel based on its drainage area. Second, Manning's equation was used to estimate the average channel depth on the basis of the bankfull discharge, the average channel width, and a Manning's n of 0.04. We used estimates for bankfull depths corresponding to the 10 yr and 25 yr floods as estimates for the average bank height. The results do not depend significantly on which interval is used, and both estimates yield bank heights comparable to those observed in the field.

Figure 3B gives the average oscillation wavelength measured for each channel (locations given in Fig. 3A) as a function of $(w_0h_0/S_0)^{1/2}$. The data points corresponding to 10 yr flow depths are plotted with circles; 25 yr flow depths are plotted with triangles. The agreement between the observed and predicted trend in the data is quite good, and provides validation for the quantitative prediction of the nonlinear model.

ACKNOWLEDGMENTS

This work was supported by National Science Foundation grant EAR-0309518. We thank Doug Hirschberg for geographic information system technical assistance. A. Brad Murray, J. Ramon Arrowsmith, and an anonymous reviewer provided helpful comments.

REFERENCES CITED

Begin, Z.B., Meyer, D.F., and Schumm, S.A., 1981, Development of longitudinal profiles of alluvial channels in response to base-level lowering: Earth Surface Processes and Landforms, v. 6, p. 49–68.

Bull, W.B., 1979, Threshold of critical power in streams: Geological Society of America Bulletin, v. 90, p. 453–464.

Bull, W.B., 1997, Discontinuous ephemeral streams: Geomorphology, v. 19, p. 227–276.

Cooke, R.U., and Reeves, R.W., 1976, Arroyos and environmental change in the American Southwest: Oxford, Clarendon Press, 213 p.

Dade, W.B., and Friend, P.F., 1998, Grain size, sediment transport regime, and channel slope in alluvial rivers: Journal of Geology, v. 106, p. 661–675.

Field, J., 2001, Channel avulsion on alluvial fans in southern Arizona: Geomorphology, v. 37, p. 93–104.

House, P.K., Pearthree, P.A., and Vincent, K.R., 1991, Flow patterns, flow hydraulics, and flood-hazard implications of a recent extreme alluvial-fan flood in southern Arizona: Geological Society of America Abstracts with Programs, v. 23, no. 5, p. 121.

Packard, F., 1974, The hydraulic geometry of a discontinuous ephemeral stream on a bajada near Tucson, Arizona [Ph.D. thesis]: Tucson, University of Arizona, 127 p.

Pima Association of Governments, 2000, Digital DTM data: http://www.pagnet.org/RDC.

Press, W.H., Flannery, B.P., and Teukolsky, S.A., 1992, Numerical recipes in C (second edition): New York, Cambridge University Press, 400 p.

Reid, I., 1994, River landforms and sediments: Evidence of climatic change, *in* Abrahams, A.D., and Parsons, A.J., eds., Geomorphology of desert environments: London, Chapman and Hall, p. 571–592.

Schumm, S.A., and Hadley, R.F., 1957, Arroyos and the semiarid cycle of erosion: American Journal of Science, v. 255, p. 161–174.

Sinha, S.K., and Parker, G., 1996, Causes of concavity in longitudinal profiles of rivers: Water Resources Research, v. 32, p. 1417–1428.

Slingerland, R.L., and Snow, R.S., 1987, Mathematical modeling of graded river profiles: Journal of Geology, v. 95, p. 15–33.

Thomas, B.E., Hjalmarson, H.W., and Waltemeyer, S.D., 1997, Methods for estimating magnitude and frequency of floods in the southwestern United States: U.S. Geological Survey Water Supply Paper 2433, 195 p.

Manuscript received 29 January 2004
Revised manuscript received 13 April 2004
Manuscript accepted 18 April 2004

Printed in USA